# Surface Organometallic Chemistry on Metals. Evidence for a New Surface Organometallic Material, $Rh[Sn(n\text{-}C_4H_9)_x]_y/SiO_2$, Obtained by Controlled Hydrogenolysis of $Sn(n\text{-}C_4H_9)_4$ on a $Rh/SiO_2$ Catalyst

**B. Didillon,† C. Houtman,‡ T. Shay, J. P. Candy,*,‡ and J. M. Basset*,‡**

*Contribution from Laboratoire COMS, E.P. C.N.R.S.48, Ecole Supérieure de Chimie Industrielle de Lyon, 43 bd du 11 Novembre 1918, 69100 Villeurbanne, France, and Institut Français du Pétrole Tet4 av. de Bois-Préau, 92506 Rueil-Malmaison, France*

*Received December 11, 1992. Revised Manuscript Received April 14, 1993**

**Abstract:** Selective hydrogenolysis of $Sn(n\text{-}C_4H_9)_4$ on a $Rh/SiO_2$ catalyst has been carried out at various temperatures and at various coverages of the metallic surface. The surface reaction and the characterization of the grafted organotin complex have been followed by analytical methods, temperature-programmed reaction, electron microscopy, XPS, IR, Mössbauer spectroscopy, $^{13}C$ CP–MAS solid-state NMR. At room temperature and in the absence of metallic Rh, $Sn(n\text{-}C_4H_9)_4$ is simply physisorbed on the silica surface and can be easily extracted. In the presence of metallic Rh, and provided that the amount of Sn introduced represents less than a monolayer on the metallic surface, the hydrogenolysis of $Sn(n\text{-}C_4H_9)_4$ occurs exclusively on the Rh particle. Only a $^{13}C$ NMR signal corresponding to $\equiv SiOSn(n\text{-}C_4H_9)_3$ was observed on the silica surface when the amount of Sn introduced was higher than ca. one monolayer on the Rh particle. Sn remains on this metallic phase even after hydrogenolysis, as demonstrated by STEM-EDAX experiments. Gas-phase evolution (TPR) and infrared studies show that the hydrogenolysis proceeds by a stepwise cleavage of Sn–alkyl bonds. For low $Sn/Rh_s$ ratios (<0.5) the reaction is continuous with formation of surface tin alkyl complexes with various degrees of substitution. For higher $Sn/Rh_s$ ratios, there is formation of a well-defined and relatively stable surface organometallic fragment which can be formulated as $Rh_s[Sn(n\text{-}C_4H_9)_2]_y$. Various possible structures have been proposed, taking into account the various results. Whereas $Rh_s[Sn(n\text{-}C_4H_9)_2]_y$ is the simplest possible model for this stable surface organometallic fragment, the results of molecular modeling seem to rule out such a model (at least at high coverages) on the basis of steric constraints. Another model, which apparently fits the experimental results better, corresponds to the general formula $(Rh_s)_2Sn[Sn(n\text{-}C_4H_9)_3]_2$.

## 1. Introduction

Surface organometallic chemistry (SOMC) is a relatively new field of chemistry devoted to the study of the reactivity of organometallic complexes with surfaces.[1] The complexes may be those of main group elements, transition metals, lanthanides, or actinides.[2-4] The surfaces may be those of highly divided inorganic oxides,[5,6] or zerovalent metallic particles.[7-10] In the latter case, the field is defined as surface organometallic chemistry on metals (SOMC/Metals). The nature of the metallic surface may be that of a highly dispersed metallic particle, supported or unsupported, or eventually that of a single crystal.

Surface organometallic chemistry on metals is quite different from organometallic chemical vapor deposition (OMCVD) since the reactions studied in SOMC/Metals usually concern less than a monolayer of the surface, whereas the objective of OMCVD is to build a multilayered material above a given metallic surface. However, the conclusions reached in SOMC/Metals may be of some help in understanding some aspects of OMCVD.

The reaction of an organometallic complex with the surface of a metal leads, in certain cases, to new catalytic materials which exhibit much higher activities and/or selectivities than conventionally prepared catalysts. For example, the reaction of tetra-*n*-butyltin ($Sn(n\text{-}C_4H_9)_4$) with the surfaces of group VIII metals above 573 K leads to bimetallic catalysts which exhibit very high selectivities and activities for the hydrogenolysis of the ethyl acetate to ethanol.[10-12] The high selectivity observed with these bimetallic catalysts, which are presumably alloys, has been ascribed to site isolation.[7] According to this concept, the catalytically "active" transition-metal atom is surrounded by catalytically "inactive" Sn atoms so that no possibility of side reactions (for example those involving dimetallacycle intermediates[13]) can occur. However, the degree of control of the coordination sphere of the active metal atom in an alloy is limited: it is restricted to the composition of the alloy and to the nature of the so-called inactive metal. Another possible objective of SOMC/Metals is to control at an atomic or molecular level the coordination sphere of the active metal with an organometallic fragment. By changing "at will" the steric and electronic

* Authors to whom correspondence should be addressed.
† Laboratoire COMS.
‡ Institut Français du Pétrole.
• Abstract published in *Advance ACS Abstracts*, September 1, 1993.

(1) *Surface Organometallic Chemistry: Molecular Approaches to Surface Catalysis*; Basset, J. M., Gates, B. C., Candy, J. P., Choplin, A., Quignard, F., Leconte, M., Santini, C. C., Eds.; Kluwer: Dordrecht, 1988.
(2) Miura, H.; Tagushi, H.; Sugiyama, K.; Matsuda, T.; Gonzalez, R. D. *J. Catal.* **1990**, *124*, 194.
(3) Yermakov, Y.; Kuznetzov, B. N.; Ryndin, Y. *J. Catal.* **1976**, *42*, 73.
(4) Izumi, Y.; Asakura, K.; Iwasawa, I. *J. Catal.* **1991**, *127*, 631.
(5) Basset, J. M.; Candy, J. P.; Choplin, A.; Santini, C. C.; Théolier, A. *Catal. Today* **1989**, *6*, 1–26.
(6) Théolier, A.; Custodero, E.; Choplin, A.; Basset, J. M.; Raatz, F. *Angew. Chem., Int. Ed. Engl.* **1990**, *29*, 805.
(7) El Mansour, A.; Candy, J. P.; Bournonville, J. P.; Ferretti, O. A.; Basset, J. M. *Angew. Chem., Int. Ed. Engl.* **1989**, *28*, 347.
(8) Agnelli, M.; Louessard, P.; El Mansour, A.; Candy, J. P.; Bournonville, J. P.; Basset, J. M. *Catal. Today* **1989**, *6*, 63.
(9) Margitfalvi, J.; Hegedus, M.; Göbölos, S.; Tálas, E. K.; Szedlacsek, P.; Szabo, S.; Nagy, F. *Proceedings of the 8th International Congress on Catalysis*; Dechema: Frankfurt-an-Main, 1984, Vol. IV; p 903.
(10) Travers, C.; Bournonville, J. P.; Martino, G. *Proceedings of the 8th International Congress on Catalysis*; Dechema: Frankfurt-an-Main, 1984; Vol. IV, p 891.
(11) Candy, J. P.; Ferretti, O. A.; Mabilon, G.; Bournonville, J. P.; El Mansour, A.; Basset, J. M.; Martino, G. *J. Catal.* **1988**, *112*, 210.
(12) Ferretti, O. A.; Bournonville, J. P.; Mabilon, G.; Martino, G.; Candy, J. P.; Basset, J. M. *J. Mol. Catal.* **1991**, *67*, 283.
(13) Eloy, R.; Leconte, M.; Basset, J. M.; Tanaka, K.; Tanaka, K.-I. *J. Am. Chem. Soc.* **1988**, *110*, 275.

0002-7863/93/1515-9380$04.00/0 

properties of the organometallic fragment, it should be possible to influence and control the chemo-, regio-, and/or stereoselectivity of a variety of reactions catalyzed by metallic surfaces, often with a selectivity which is unpredictable or not easily controlled. In order to achieve this goal, it is necessary to develop a new aspect of surface organometallic chemistry on metals: grafting of stable organometallic fragments onto the surface of zerovalent metal particles followed by a study of their structure, stability, and reactivity.

This article reports results which demonstrate, for the first time, that it is possible to graft organometallic fragments, namely $Sn(n\text{-}C_4H_9)_x$, onto the surface of Rh particles supported on silica. These organometallic fragments are obtained by selective hydrogenolysis of $Sn(n\text{-}C_4H_9)_4$ on metallic Rh and are thermally stable on the particle up to a temperature of ca. 423 K. As already proposed in a preliminary communication,[14] the presence of the Sn fragment on the surface of Rh completely reverses the chemoselectivity of this metal in the hydrogenation of $\alpha,\beta$-unsaturated aldehydes. Whereas Rh on silica exhibits some degree of selectivity for the reduction of the conjugated C=C double bond, the same surface modified by an organostannic fragment becomes fully selective for the reduction of the C=O double bond.

## 2. Experimental Section

**2.1. Monometallic Supported Rh Catalyst.** The monometallic catalyst preparation has been described elsewhere.[15] The silica support (Aerosil 200 $m^2\ g^{-1}$) was purchased from Degussa. The Rh was grafted onto silica by cationic exchange between $[RhCl(NH_3)_5]^{2+}$ ions and surface $\equiv SiO^-NH_4^+$ groups. The surface complex obtained was decomposed by calcination at 673 K in flowing nitrogen/oxygen (5/1), reduced in flowing $H_2$ at 673 K, and then "passivated" at 298 K under dry air. The Rh and Cl loadings were 1.1% and 0.06% by weight, respectively.

**2.2. Chemisorption Measurements.** These experiments were carried out using conventional static volumetric equipment as already described.[15] The vacuum was achieved by means of a pump, and the equilibrium pressure was measured with a Texas Instrument gauge (pressure range 0–1000 mbar, accuracy 0.1 mbar). The gas phase was extracted from the vessel and then analyzed by means of a mass spectrometer (Supravac from Vacuum Generator) or by gas chromatography (GC).

**2.3. Temperature-Programmed Reaction (TPR) between $Sn(n\text{-}C_4H_9)_4$ and Reduced Rh Particles ($Rh_s$-$H/SiO_2$).** This reaction was performed in the same apparatus as before.[15] A given amount of the monometallic supported Rh catalyst was loaded in the reactor, reduced at 623 K under $H_2$, and then stabilized at room temperature under 20 mbar of $H_2$. This catalyst is described as $Rh_s$-H catalyst from here on. The desired amount of $Sn(n\text{-}C_4H_9)_4$ was then carefully introduced into the reactor via a septum without any contact with air. The reaction was performed by increasing the temperature of the reactor from 298 K to 673 K in steps of 50 K. Each step was maintained for 0.5 h. The gases evolved during the reaction were trapped at liquid nitrogen temperature in another part of the apparatus, to avoid possible feedback of the gases onto the catalytic surface and further hydrogenolysis. After each step, the gas phase was analyzed by GC, mass spectrometry (MS), and volumetric measurements.

**2.4. Electron Microscopy (CTEM and STEM).** Conventional transmission electron microscopy (CTEM) and scanning transmission electron spectroscopy (STEM) were performed with use of JEOL 100 CX and Vacuum Generator HB5 electron microscopes, respectively. CTEM was used to obtain histograms of the metallic particle size of the catalysts. STEM experiments were carried out to locate Sn and Rh on the surface.

**2.5. Infrared Spectroscopy.** Infrared spectra were obtained with a Nicolet 10 MX-1 Fourier transform instrument. The samples were placed in a sample holder which could move inside a closed reactor from the treatment position (located in an oven) to the analysis position (located in between two $CaF_2$ windows in the infrared beam). The reactor could be evacuated or filled with a known pressure of gas. CO adsorption bands were recorded as the difference between the IR spectra of bare and CO-covered samples. Infrared spectroscopy was also used to evaluate the number of alkyl groups present on the surface during reaction of $Rh_s/SiO_2$ with $Sn(n\text{-}C_4H_9)_4$.

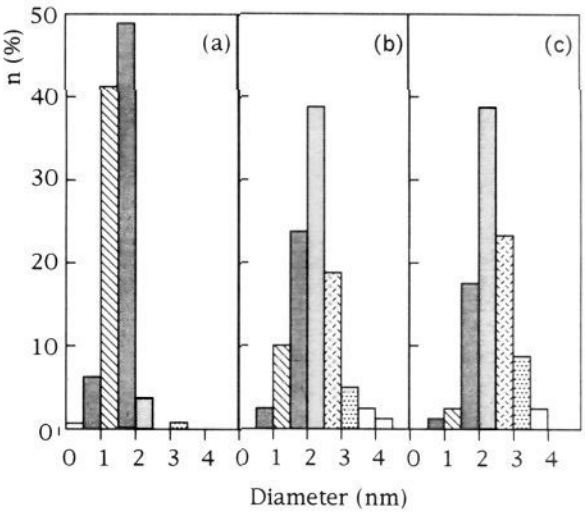


**Figure 1.** Particle size distribution of the various catalysts deduced from CTEM: (a) $Rh/SiO_2$, (b) $Rh_s[Sn(n\text{-}C_4H_9)_2]/SiO_2$, (c) $RhSn/SiO_2$.

**2.6. XPS Analysis.** X-ray photoelectron spectra were obtained with an HP 59 50a spectrometer. The instrument was calibrated with the Si $2p_{3/2}$ core level spacing of 103.4 eV. The samples were loaded onto a holder which could be removed from a treatment position (where the catalyst can be treated under controlled atmosphere at temperatures between 300 and 700 K) to an analysis room. The different bimetallic catalysts were prepared in situ to prevent all contamination of solids by air.

**2.7. Mössbauer Spectroscopy.** Mössbauer studies were performed with a constant acceleration spectrometer using a $Ca^{119}SnO_3$ source. All isomer shifts were referred to $CaSnO_3$ and $Sn^{(0)}$. A standard least-squares minimization routine was used to fit the spectra as a superposition of Lorentzian lines. The uncertainties in isomer shift ($\delta$) and quadrupole splitting ($\Delta$) measurements are respectively about 0.03 and 0.02 mm $s^{-1}$. The Mössbauer spectra of the samples were recorded at liquid nitrogen temperature. The catalyst was prepared following the procedure used for the reaction between $Sn(n\text{-}C_4H_9)_4$ and $Rh_s$-$H/SiO_2$ (see above) up to the desired temperature. The sample (200-mg pellets) was placed between two "Dural" circular plates used as a sample holder. The two plates were then stuck together. All these experiments were performed without any contact with air, in a glove box under argon. The sample holder was then placed in the Mössbauer apparatus and frozen at liquid nitrogen temperature.

**2.8. $^{13}C$ CP-MAS Solid-State NMR.** A Bruker MSL 300 multinuclear spectrometer was used for $^{13}C$ NMR experiments. The resonance frequency was 75.47 MHz. The spectrometer was equipped with a ball bearing system which permits the rotation of the rotor at ca. 4 kHz. All samples were handled under a pure argon stream and transferred to the rotor in a glovebag under argon.

**2.9. Molecular Modeling.** Metallic particle size was modeled assuming a cubooctahedral shape.[16] Steric hindrance for Sn complexes grafted on the metallic surface $\{Rh_s[Sn(n\text{-}C_4H_9)_x]_y\}$ was calculated by using SYBYL molecular modeling software from TRIPOS and VAX 3100 with Evans and Sutherland PS390 as hardware. We used the classical Tripos[17] force field data for H and C. Bond distances, angles, and constants not found in the Tripos force field were based on literature values.[17]

## 3. Results

**3.1. Characterization of the Monometallic Materials: $Rh/SiO_2$. 3.1.1. Electron Microscopy (CTEM).** The particle size

(14) Didillon, B.; Candy, J. P.; El Mansour, A.; Houtman, C.; Basset, J. M. *J. Mol. Catal.* **1992**, *74*, 43.

(15) Candy, J. P.; Ferretti, O. A.; El Mansour, A.; Mabilon, G.; Bournonville, J. P.; Basset, J. M.; Martino, G. *J. Catal.* **1988**, *112*, 201.

(16) Van Hardeveld, R.; Hartog, F. *Surf. Sci.* **1969**, *15*, 189.

(17) (a) Tripos Associates, 1699 S. Hanley Road, Suite 303, St. Louis, MO, 63144; Sybyl 5.5 (1992). (b) Wells, A. F. *Structural Inorganic Chemistry*; Clarence: Oxford, 1986; p 289. (c) Boeyens, J. C. A.; Cotton, F. A.; Han, S. *Inorg. Chem.* **1985**, *24*, 1750. (d) Allinger, N. L.; Quinn, M. I.; Chen, K.; Thompson, B.; Frierson, M. R. *J. Mol. Struct.* **1989**, *194*, 1. (e) Clark, M.; Cramer, R.; Opdenbosch, N. *J. Comp. Chem.* **1989**, *10*, 982. (f) Burket, V.; Allinger, N. L. *Molecular Mechanisms*; ACS Monograph No. 177, American Chemical Society: Washington, DC, 1982.

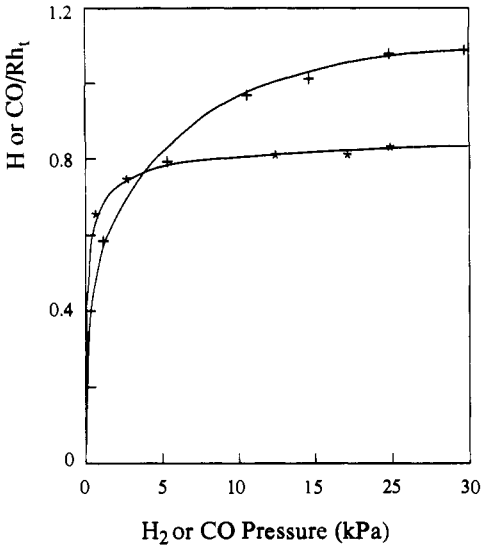


**Figure 2.** Isotherms of CO (+) and $H_2$ (*) adsorption on the starting Rh catalyst.

distribution of the $Rh/SiO_2$ catalyst has been determined by CTEM analysis. A typical histogram is given in Figure 1. Thedistribution is rather narrow, with an average diameter of 1.4 nm. If the particles are assumed to have a cubooctahedral shape,[16] this corresponds to a dispersion of close to 0.75.

**3.1.2. Chemisorption of CO and $H_2$.** Chemisorption of CO and $H_2$ was used as an indirect method to determine metal particle size. The isotherms of chemisorption for CO and $H_2$ were measured at 298 K as shown in Figure 2. Both isotherms show a plateau, at equilibrium pressures of 10 kPa of CO and 30 kPa of $H_2$, respectively. For CO, the amount of adsorbed gas was corrected for the amount of gas adsorbed on the support. The accepted stoichiometries, 1.2 for $H/Rh_s$[15,21] and 1 for $CO/Rh_s$,[18] were assumed at the above-mentioned equilibrium pressures. The resulting dispersion, 0.8, is in good agreement with the values obtained by CTEM. For a Rh dispersion of 0.8, we obtain the same $H/Rh_s$ ratio as found by Kip et al.[21]

**3.1.3. X-ray Photoelectron Spectroscopy (XPS).** XPS analysis of the reduced sample confirms that all the Rh atoms are fully reduced. Only the binding energies at 311.5 eV (for $3d_{3/2}$) and 307.0 eV (for $3d_{5/2}$) are observed, and are in good agreement with values obtained for Rh metal (Table I).

**3.1.4. Infrared Spectroscopy of Adsorbed CO.** CO has also been used as a molecular probe to characterize the metallic phase. IR experiments were carried out on a reduced Rh sample which was exposed to CO at room temperature. The resulting IR spectrum is typical of CO adsorbed on a fully-reduced Rh particle, with two main bands at 2059 and 1866 $cm^{-1}$ (Figure 3a). The narrow peak at 2059 $cm^{-1}$ has already been ascribed to the linear form of coordinated CO, while the broader band at 1866 $cm^{-1}$ is usually attributed to the multiply-bonded ($\mu_{-2}$ or $\mu_{-3}$) forms of CO coordinated to two or three Rh atoms ("bridging CO").[22-30] The absence of any detectable bands at 2080 and 2020 $cm^{-1}$,

**Table I.** XPS Analysis of $Pr/SiO_2$ and $Rh_s[Sn(n\text{-}C_4H_9)_x]_y$ Samples: Binding Energies (eV) of Rh ($3d_{3/2}$, $3d_{5/2}$) and Sn ($3d_{3/2}$, $3d_{5/2}$) Electrons

| samples | Rh $3d_{3/2}$ | Rh $3d_{5/2}$ | Sn $3d_{3/2}$ | Sn $3d_{5/2}$ |
|---|---|---|---|---|
| $Rh_2O_3$[a] | 313.2 | 308.5 | | |
| Rh(0) metal[a] | 311.5 | 307.0 | | |
| $SnO_2$[a] | | | 494.9 | 486.4 |
| SnO[a] | | | 494.6 | 486.1 |
| Sn metal[a] | | | 493.2 | 484.7 |
| $Sn(n\text{-}C_4H_9)_4$[a] | | | 494.7 | 486.2 |
| $Rh/SiO_2$[b] | 311.7 | 307.0 | | |
| $Rh_s[Sn(n\text{-}C_4H_9)_x]_y$[c] | | | 495.0 | 486.5 |
| $Rh_s[Sn(n\text{-}C_4H_9)_x]_y$[d] | 311.7 | 307.0 | 495.4 | 486.6 (75%) |
| | | | 493.5 | 484.8 (25%) |
| RhSn[e] | 311.7 | 307.0 | 493.5 | 485.0 |

[a] Data from ref 39. [b] Monometallic material treated under $H_2$ at 623 K. [c] After reaction at 323 K ($y$ ca. 1). [d] After ($c$) and then 373 K. [e] After ($d$) and the 573 K.

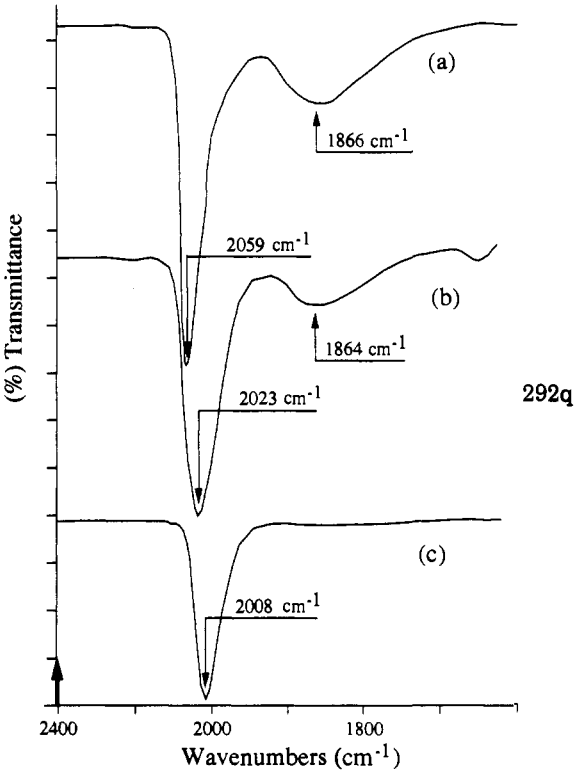


**Figure 3.** IR spectra of CO adsorbed on (a) $Rh(0)/SiO_2$, (b) $Rh_s[Sn(n\text{-}C_4H_9)_2]_y/SiO_2$, and (c) Rh–Sn alloy.

which correspond to the species $Rh^I(CO)_2$, confirms that the Rh atoms are totally reduced and that there are no unreduced isolated $Rh^I$ organometallic fragments on the silica support.[24,25]

The above characterization of the starting monometallic particles indicates that the Rh is fully reduced, with an average particle size of 1.4 nm, and exhibits all the characteristics (chemical and physical) of well-dispersed metal particles.

**3.2. Interaction between $Sn(n\text{-}C_4H_9)_4$ and the Silica Surface in the Absence of Metallic Rh.** It has been reported[31,32] that under certain conditions $Sn(n\text{-}C_4H_9)_4$ reacts with the silanol

(18) Wanke, S. D.; Dougharty, N. A. *J. Catal.* **1972**, *24*, 367.
(19) Koningsberger, D. C.; van Zon, J. B. A. D.; van't Blik, H. F. J.; Visser, G. J.; Prins, R.; Mansour, A. N.; Sayers, D. E.; Short, D. R.; Katzer, J. R. *J. Phys. Chem.* **1985**, *89*, 4075.
(20) Van Zon, J. B. A. D.; Koningsberger, D. C.; Van't Blik, H. F. J.; Sayers, D. E. *J. Chem. Phys.* **1985**, *82*, 5742.
(21) Kip, B. J.; Duivenvoorden, F. B. M.; Koningsberger, D. C.; Prins, R. *J. Am. Chem. Soc.* **1986**, *108*, 5633; *J. Catal.* **1987**, *105*, 26.
(22) Yang, A. C.; Garland, C. W. *J. Phys. Chem.* **1957**, *61*, 1504.
(23) Yates, J. T.; Duncan, T. M.; Worley, S. D.; Vaugham, R. W. *J. Chem. Phys.* **1979**, *70*, 1219.
(24) Rice, C. A.; Worley, S. D.; Curtis, C. W.; Guin, J. A.; Tarrer, A. R. *J. Chem. Phys.* **1981**, *74*, 6487.
(25) Worley, S. D.; Rice, C. A.; Mattson, G. A.; Curtis, C. W.; Guin, J. A.; Tarrer, A. R. *J. Chem. Phys.* **1982**, *76*, 20; *J. Phys. Chem.* **1982**, *86*, 2714.
(26) Primet, M.; Vedrine, J. C.; Naccache, C. *J. Mol. Catal.* **1978**, *4*, 411.
(27) Smith, A. K.; Hugues, F.; Théolier, A.; Basset, J. M.; Hugo, R.; Zanderighi, G. M.; Bilhou-Bougnol, V.; Grazydon, W. F. *Inorg. Chem.* **1979**, *18*, 3104.
(28) Watters, K. W.; Howe, R. F.; Chojnacki, T. P.; Fu, C. M.; Schneider, R. L.; Wong, N. B. *J. Catal.* **1980**, *66*, 424.
(29) Worley, S. D.; Rice, C. A.; Mattson, G. A.; Curtis, C. W.; Guin, J. A.; Tarrer, A. R. *J. Chem. Phys.* **1982**, *76*, 20.
(30) Kraus, L.; Zaki, M. I.; Knözinger, H. J. *J. Mol. Catal.* **1989**, *55*, 55.
(31) Nédez, C. Ph.D. Thesis, University of Lyon 1, 1992.
(32) Nédez, C.; Theolier, A.; Lefebvre, F.; Choplin, A.; Basset, J. M.; Joly, J. F. *J. Am. Chem. Soc.* **1993**, *115*, 722.

**Table II.** CP-MAS $^{13}C$ NMR Chemical Shifts (ppm) for Various Molecular and Surface Organotin Compounds[a]

| sample | $C_\alpha$ | $C_\beta$ | $C_\gamma$ | $C_\delta$ |
|---|---|---|---|---|
| $Sn(n\text{-}C_4H_9)_4$ (liquid phase) | 9.1 | 29.6 | 27.6 | 13.7 |
| $SiO_2 + Sn(n\text{-}C_4H_9)_4$ (298 K) | 7.8 | 28.5 | 25.6 | 12.6 |
| $\equiv SiO[Sn(n\text{-}C_4H_9)_3]$[33] | 15.2 | 26.7 | 26.7 | 11.3 |
| $Rh_s[Sn(n\text{-}C_4H_9)_2]_{0.8}/SiO_2$ | n.d. | n.d. | n.d. | n.d. |
| $Rh_s[Sn(n\text{-}C_4H_9)_2]_1/SiO_2$ | n.d. | ~29 | ~29 | n.d. |
| $Rh_s[Sn(n\text{-}C_4H_9)_2]_{1.5}/SiO_2$ | 15.3 | ~27 | ~27 | 11.3 |

[a] n.d. = no detectable signal.

groups of silica to give a well-defined surface complex according to reaction I:

$$\equiv SiOH + Sn(n\text{-}C_4H_9)_4 \rightarrow \equiv SiOSn(n\text{-}C_4H_9)_3 + n\text{-}C_4H_{10} \quad (I)$$

The trisalkyltin surface species was characterized by several analytical methods, including $^{119}Sn$, $^{13}C$ CP–MAS solid-state NMR (Table II), microanalysis, and IR spectroscopy. Reaction I occurs if $Sn(n\text{-}C_4H_9)_4$ is allowed to react in a closed vessel, for several hours, with a silica surface previously degassed at ca. 773 K.

However, if the experimental conditions are changed so that there is a cold trap to remove any unreacted $Sn(n\text{-}C_4H_9)_4$, there is no measurable reaction with the silica support above 373 K. Below 373 K, the $Sn(n\text{-}C_4H_9)_4$ is only physisorbed on the silica surface and can be easily trapped on a cold finger prior to any reaction with the surface. Additionally, chemical analysis of a sample obtained by reaction (up to 573 K) between the silica support and a quantity of $Sn(n\text{-}C_4H_9)_4$ introduced corresponding to 2 wt % Sn per gram of silica gave only a minor quantity of fixed Sn equal to 0.06 wt %. GC analysis of the gases evolved during TPR between the silica surface and $Sn(n\text{-}C_4H_9)_4$, did not show any detectable amount of butane or lower hydrocarbons, confirming the absence of any significant reaction between the $Sn(n\text{-}C_4H_9)_4$ and the silica support under our experimental conditions.

**3.3. Interaction between $Sn(n\text{-}C_4H_9)_4$ and $Rh_s\text{-}H/SiO_2$.** The reaction between $Sn(n\text{-}C_4H_9)_4$ and $Rh_s\text{-}H/SiO_2$ was carried out by introducing a given amount of $Sn(n\text{-}C_4H_9)_4$ on the reduced catalyst in the presence of 30 mbar of $H_2$. The amount of complex introduced was calculated so as to correspond to an overall ratio of $Sn/Rh_s$ less than unity.

**3.3.1. Temperature-Programmed Reaction (TPR).** The reaction between $Sn(n\text{-}C_4H_9)_4$ and the $Rh_s\text{-}H/SiO_2$ catalyst was followed by qualitative and quantitative analysis of the various gases (mostly ethane, butane, and butenes) evolved during the TPR study. The amount of $Sn(n\text{-}C_4H_9)_4$ introduced was calculated so that the ratio of Sn introduced per surface Rh atom was varied between ca. 0.3 and 1. The results are shown in Tables III and IV.

Analysis of these data shows various aspects of the hydrogenolysis of the organometallic fragment at the Rh surface: After reaction at 373 K, the percentage of C remaining on the surface corresponds to an average value of approximately two butyl groups per fixed Sn (Table III). Reaction at temperatures greater than 373 K causes the entire amount of Sn introduced to remain fixed on the solid. Above 523 K, the ratio of $C_4$ evolved per mole of fixed Sn is close to 4 regardless of the ratio of $Sn/Rh_s$, since all the butyl groups of $Sn(n\text{-}C_4H_9)_4$ have undergone hydrogenolysis.

The quantity of gas (reported as $C_4$ equivalents) evolved during the TPR study was dependent on the $Sn/Rh_s$ ratio. When this ratio is lower than 0.6, the hydrogenolysis of $Sn(n\text{-}C_4H_9)_4$ is a continuous process without any apparent discontinuities. Above 0.6, a plateau is clearly observed between 373 and 423 K (Figure 4). In the temperature range corresponding to this plateau, the number of butyl groups remaining on the surface is ca. 2 $C_4/Sn$, which is in agreement with the chemical analysis (Table III). The presence of a plateau indicates that an organometallic fragment is thermally stable in the corresponding range of temperature. In the following sections of the paper, we will describe this new material by the general formula $Rh_s[Sn(n\text{-}C_4H_9)_x]_y$.

Another aspect of the hydrogenolysis of $Sn(n\text{-}C_4H_9)_4$ concerns the nature of the gaseous products evolved during this reaction (Table IV). At ratios of $Sn/Rh_s$ lower than ca. 0.6, ethane and butane are the main products of the reaction at any temperature. Rh is a known catalyst for the selective hydrogenolysis of *n*-butane to ethane.[33] Ethane may be a primary product from the hydrogenolysis of the *n*-butyl ligands still coordinated to Sn atoms or a secondary product from the hydrogenolysis of *n*-butane. The latter reaction most likely occurs on Rh sites which are not poisoned by Sn atoms. At ratios of $Sn/Rh_s$ higher than ca. 0.6, ethane is no longer observed, indicating that the remaining Rh sites have probably been poisoned by Sn atoms and/or Sn organometallic fragments. At ratios of $Sn/Rh_s$ equal to ca. 0.7, butane is the major product of the reaction, indicating that the Sn-modified Rh surface still preserves some hydrogenolysis properties toward Sn–C bonds. At ratios of $Sn/Rh_s$ equal to 1, butene is observed above 523 K. The butane/butene ratio of ca. 1 suggests that either a dismutation process occurs between two adjacent butyl ligands (via a $\beta$-hydrogen transfer mechanism) or the metallic surface has lost some of its C=C hydrogenation properties.

**3.3.2. Infrared Spectroscopy.** Infrared spectroscopy was used to follow the hydrogenolysis of $Sn(n\text{-}C_4H_9)_4$ with the catalyst $Rh_s\text{-}H/SiO_2$ (Figure 5). Room temperature adsorption of $Sn(n\text{-}C_4H_9)_4$ onto the $Rh_s\text{-}H/SiO_2$ catalyst strongly modifies the $\nu$(OH) vibrations of the silica support, which are initially situated at 3745 $cm^{-1}$. After adsorption of $Sn(n\text{-}C_4H_9)_4$ at room temperature, the silanol band decreases in intensity and a new broad peak appears at 3698 $cm^{-1}$. The new peak is believed to be due to hydrogen bonding between the silanol groups and the alkyl groups of the $Sn(n\text{-}C_4H_9)_4$ which has been adsorbed onto the support. This type of hydrogen bonding has been previously observed by infrared spectroscopy and $^{13}C$ CP–MAS NMR.[32] Treatment of the solid above 373 K causes the frequency and intensity of the $\nu$(OH) bands of the starting silica to be fully restored, whereas the broad peak at 3698 $cm^{-1}$ totally disappears. Simultaneously, the $\nu$(C–H) bands corresponding to the grafted alkyl chains are still observed at 2958 $\nu(CH_3)_a$, 2924 $\nu(CH_2)_a$, 2872 $\nu(CH_3)_s$, and 2855 $cm^{-1}$ $\nu(CH_2)_s$.[34] These results indicate that when reduced metallic Rh particles are present on silica, $Sn(n\text{-}C_4H_9)_4$ reacts with the metal particles preferentially.

**3.3.3. $^{13}C$ CP–MAS Solid-State NMR.** $^{13}C$ CP–MAS solid-state NMR was used to try to characterize the grafted organometallic fragment. Since it is possible to graft $Sn(n\text{-}C_4H_9)_4$ on silica as $\equiv SiOSn(n\text{-}C_4H_9)_3$, the chemical shifts of this grafted complex as well as those of $Sn(n\text{-}C_4H_9)_4$ were used as standards. When $Sn(n\text{-}C_4H_9)_4$ was adsorbed at room temperature on a $Rh_s\text{-}H/SiO_2$ catalyst, the peaks observed were almost identical with those of liquid $Sn(n\text{-}C_4H_9)_4$ (Table II). This confirms the physisorption of $Sn(n\text{-}C_4H_9)_4$ on the surface.

After reaction at the temperature needed to form the surface complex $Rh_s[Sn(n\text{-}C_4H_9)_2]_y$ (see section 3.3.1.), the results observed depend on the value of "*y*". For a $Sn/Rh_s$ ratio ($y$) lower than 1, the $^{13}C$ NMR signal totally disappears. However, if this ratio is higher than 1.5, a weak signal is observed which is identical with that obtained for the surface complex $\equiv SiOSn(n\text{-}C_4H_9)_3$.[32] This is in agreement with the infrared spectroscopy study (see section 3.3.2), which shows that hydrogenolysis of $Sn(n\text{-}C_4H_9)_4$ occurs preferentially on the metallic surface. Above a certain value, which is probably close to the saturation of the

(33) Holgado, M. J.; Rives, V. *J. Mol. Catal.* **1990**, *63*, 353.
(34) Marchand, A.; Forel, M. T.; Lebedeff, M.; Valade, J. *J. Organomet. Chem.* **1971**, *26*, 69.

**Table III.** Relative Amounts of $Sn(n\text{-}C_4H_9)_4$ Introduced and Relative Amounts of $C_4$ Hydrocarbons Evolved during the Reaction with $Rh_s/SiO_2$ at Different Temperatures, Compared to the Amounts of Sn and C Remaining on the Catalyst after Reaction (Chemical Analysis)

| $Sn(n\text{-}C_4H_9)_4$ introduced/$Rh_t$ | temp (K) | $C_4$ evolved/Sn[a] | Sn remaining/$Rh_t$[b] | $C_4$/Sn remaining[c] | $C_4$/Sn remaining[d] |
|---|---|---|---|---|---|
| 0.8 | 373 | 2.1 | 0.79 | 1.9 | 2.0 |
| 0.2 | 523 | 4.0 | 0.25 | 0 | <0.1 |
| 0.5 | 523 | 4.0 | 0.45 | 0 | <0.1 |
| 0.8 | 523 | 4.1 | 0.75 | 0 | <0.1 |

[a] Butyl groups evolved from the sample, by volumetric measurement. [b] Sn fixed on $Rh/SiO_2$, from chemical analysis of the sample after removal of unreacted $Sn(n\text{-}C_4H_9)_4$ by washing with *n*-heptane. [c] Butyl groups remaining on the catalyst (deduced from the quantity of $C_4$ evolved). [d] Butyl groups remaining on the sample, from chemical analysis.

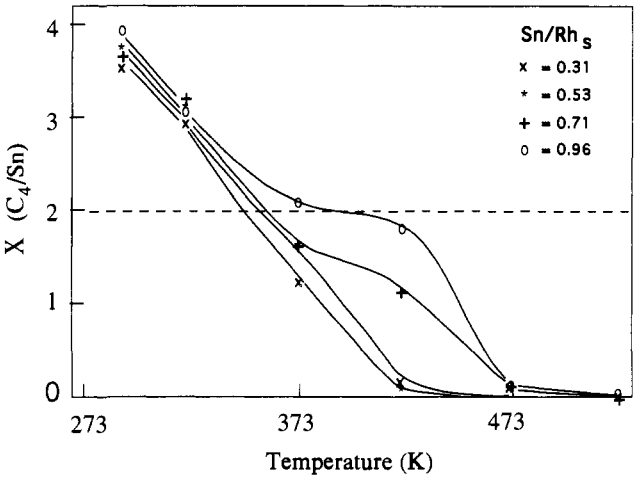


**Figure 4.** Number ($X$) of butyl groups per Sn remaining on the surface for each temperature and for various values of $y$ (ratios of $Sn/Rh_s$). The numbers are deduced from the data in Table III.

**Table IV.** Gases Evolved during the Reaction between Various Amounts of $Sn(n\text{-}C_4H_9)_4$ and a Constant Amount of $Rh_s\text{-}H/SiO_2$ at Increasing Temperatures

| | | amount of gas evolved (mmol/g)[b] | | | | | | |
|---|---|---|---|---|---|---|---|---|
| $Sn/Rh_s$[a] | gas | 298 K | 373 K | 373 K | 423 K | 473 K | 523 K | total $C_4$/Sn |
| 0.31 | $C_2H_6$ | 3.4 | 1.0 | 0.3 | 39.2 | 6.1 | 0.0 | |
| | $C_4H_8$ | 0.0 | 0.0 | 0.0 | 0.0 | 0.0 | 0.0 | |
| | $C_4H_{10}$ | 6.4 | 11.5 | 31.1 | 0.0 | 0.0 | 0.0 | |
| | $C_4$ eq. | 8.1 | 12.0 | 31.3 | 19.6 | 3.0 | 0.0 | 4.0 |
| 0.53 | $C_2H_6$ | 4.8 | 0.0 | 4.1 | 80.3 | 4.1 | 0.0 | |
| | $C_4H_8$ | 0.0 | 0.0 | 0.0 | 0.0 | 0.0 | 0.0 | |
| | $C_4H_{10}$ | 4.8 | 19.7 | 44.9 | 8.2 | 0.0 | 0.0 | |
| | $C_4$ eq. | 7.1 | 19.7 | 45.9 | 48.3 | 2.0 | 0.0 | 3.9 |
| 0.71 | $C_2H_6$ | 2.0 | 0.0 | 1.0 | 4.2 | 1.5 | 0.0 | |
| | $C_4H_8$ | 0.0 | 0.0 | 0.0 | 0.0 | 0.0 | 0.0 | |
| | $C_4H_{10}$ | 14.6 | 16.6 | 70.7 | 20.8 | 45.5 | 0.0 | |
| | $C_4$ eq. | 15.6 | 16.6 | 70.7 | 20.8 | 46.3 | 0.0 | 4.1 |
| 0.96 | $C_2H_6$ | 0.0 | 0.0 | 0.0 | 0.0 | 0.0 | 0.0 | |
| | $C_4H_8$ | 0.0 | 0.0 | 0.0 | 0.0 | 47.6 | 0.0 | |
| | $C_4H_{10}$ | 4.4 | 46.1 | 55.0 | 22.3 | 51.3 | 0.0 | |
| | $C_4$ eq. | 4.5 | 46.1 | 55.0 | 22.3 | 98.8 | 0.0 | 4.0 |

[a] $Sn/Rh_s$ is the amount of Sn remaining on the catalyst (chemical analysis). [b] Gas evolved during temperature increase of 50 K (except 298 K), followed by 1 h at the stated temperature.

metallic surface, the organotin complex then reacts or migrates onto the silica support to give the surface complex $\equiv SiOSn(n\text{-}C_4H_9)_3$.

The absence of a detectable signal corresponding to the grafted organotin complex on the metallic particle might be caused by the "Knight Shift" phenomenon, which is caused by the paramagnetism of the Rh metal particle. This phenomenon is known to broaden NMR signals and to shift resonances by several hundred ppm.[35-38]

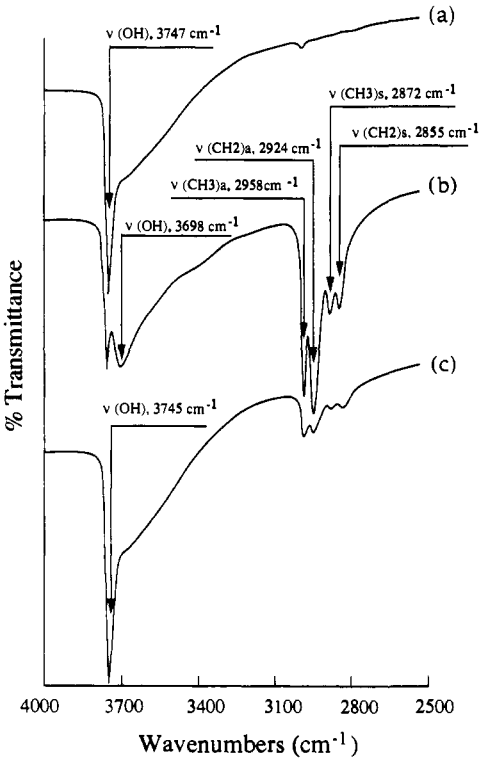


**Figure 5.** Infrared spectra during the hydrogenolysis at increasing temperatures of $Sn(n\text{-}C_4H_9)_4$ supported on Rh on silica (pretreated at 623 K for 16 h): (a) blank of $silica_{(623)}$; (b) after adsorption of $Sn(n\text{-}C_4H_9)_4$ at 300 K; (c) (b) after treatment at 373 K under 30 mbar of $H_2$.

**3.4. Characterization of $Rh_s[Sn(n\text{-}C_4H_9)_x]_y$ ($1 < x < 3$, $0 < y < 1$).** Hydrogenolysis of $Sn(n\text{-}C_4H_9)_4$ with the catalyst $Rh_s\text{-}H/SiO_2$ gives the surface complex $Rh_s[Sn(n\text{-}C_4H_9)_x]_y$ ($1 < x < 3$, $0 < y < 1$). Interestingly, the most thermally stable fragments are observed for $0.6 < y < 1$. For this range of Rh coverage, the corresponding average $x$ value was found to be equal to about 2, *as if a well-defined surface molecular structure is at the origin of this unusual thermal stability.* Additionally, the catalytic activities and selectivities in the hydrogenation of $\alpha,\beta$-unsaturated aldehydes were the highest when such a surface structure was formed.[14] Several physical techniques have been applied in order to characterize the surface organometallic complex corresponding to the average formula $Rh_s[Sn(n\text{-}C_4H_9)_2]/SiO_2$ (that is $x = 2$, $y = 1$).

**3.4.1. Electron Microscopy.** Conventional transmission electron microscopy (CTEM) of the bimetallic material $Rh_s[Sn(n\text{-}C_4H_9)_2]/SiO_2$ gives a narrow particle size distribution centered at ca. 2.2 nm (Figure 1b). This increase of average diameter (0.7 nm) compared to that of the monometallic catalyst ($Rh/SiO_2$) is consistent with the formation of no more than one or two monolayers of Sn on the Rh particles.

(35) Compton, D. B.; Root, W. T. *J. Catal.* **1992**, *136*, 199.
(36) Zilm, K. W.; Bonneviot, L.; Haller, G. L.; Hazn, O. H.; Kermarec, M. *J. Phys. Chem.* **1990**, *94*, 8495.
(37) Ansermet, J. P.; Wang, P. K.; Slichter, C. P.; Sinfelt, J. H. *Phys. Rev. B* **1988**, *37*, 1417.
(38) Shore, S. E.; Ansermet, J. P.; Slichter, C. P.; Sinfelt, J. H. *Phys. Rev. Lett.* **1987**, *58*, 953.

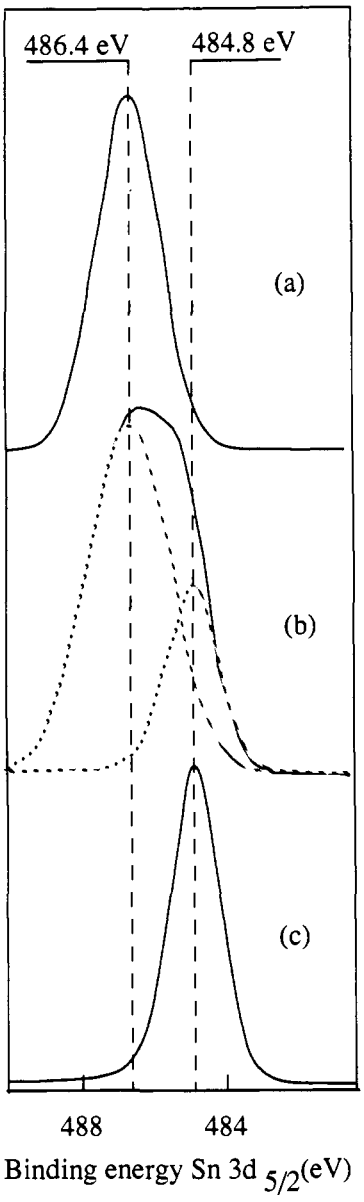


**Figure 6.** XPS spectra taken after hydrogenolysis of $Sn(n\text{-}C_4H_9)_4$ supported on $Rh/SiO_2$ at increasing temperatures: (a) 323 K; (b) 373 K; (c) 523 K.

Examination of $Rh_s[Sn(n\text{-}C_4H_9)_2]/SiO_2$ by scanning transmission electron microscopy (EDAX) was not possible because the electronic beam decomposes the organic fragments and causes a "contamination effect". Nevertheless, this is confirmation that the alkyl ligands are on the metal particle. A sample that was treated at 573 K in order to remove the alkyl groups showed a composition of Sn and Rh atoms in an atomic ratio close to 0.8 with a narrow distribution. No isolated Sn atoms on the silica surface were observed for the de-alkylated catalyst or for $Rh_s[Sn(n\text{-}C_4H_9)_2]/SiO_2$. The results from electron microscopy confirm that the organometallic fragments are situated on the Rh particle and not on the silica support.

**3.4.2. X-ray Photoelectron Spectroscopy (XPS).** XPS data obtained "in situ" on $Rh_s[Sn(n\text{-}C_4H_9)_2]/SiO_2$ are shown in Table I and Figure 6. The Rh $3d_{3/2}$ and $3d_{5/2}$ binding energies correspond to those of Sn(II) or Sn(IV). After deconvolution of the spectra, the XPS signal can be attributed to ca. 75% of Sn(II) or Sn(IV) and ca. 25% of Sn(0). After treatment under $H_2$ at 623 K, the Sn and Rh binding energies were in agreement with those of Sn(0) and Rh(0).

**3.4.3. Mössbauer Spectroscopy.** Mössbauer spectroscopy has been used to obtain information on the oxidation state of Sn in three different samples: (a) $Sn(n\text{-}C_4H_9)_4$ physisorbed on silica, (b) $Rh_s[Sn(n\text{-}C_4H_9)_2]/SiO_2$ ($x = 2$, $y = 1$), and (c) $\equiv SiOSn(n\text{-}C_4H_9)_3$. The spectra were recorded at 77 K (Figure 7 and Table V). For the three samples, the isomer shifts, $\delta$, were found to be very similar (about 1.4 mm $s^{-1}$), but the quadrupole splittings, $\Delta$, were very different (0 (a), 1.4 (b), and 2.7 mm $s^{-1}$ (c)). Clearly, the three spectra correspond to three different species, as deduced from the previous physical techniques. Comparison of the Mössbauer data with that of some molecular analogues is shown in Table V. The value of the isomer shift (related to the oxidation state of Sn) for $Rh_s[Sn(n\text{-}C_4H_9)_2]/SiO_2$ seems to be closer to those observed for Sn(IV) than those observed for Sn(II) (Table

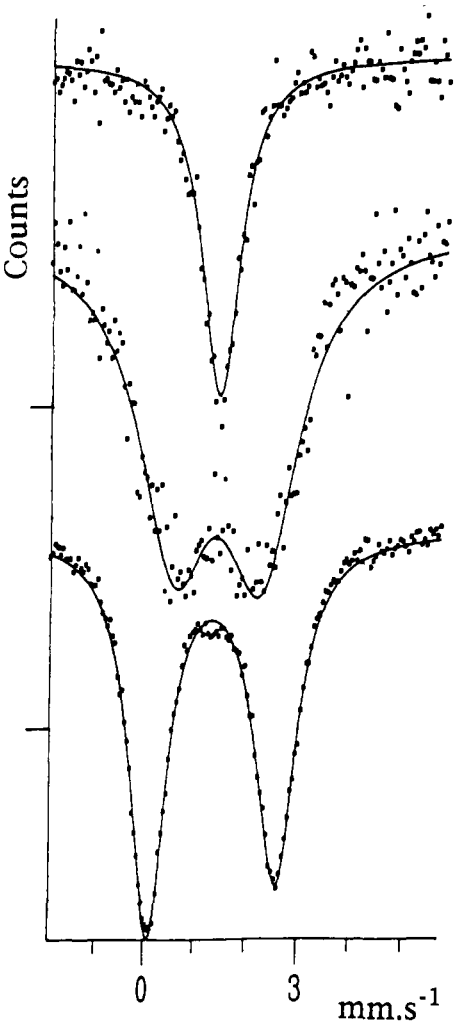


**Figure 7.** Mössbauer spectra of (a, top) $Sn(n\text{-}C_4H_9)_4$ physisorbed on silica, (b, middle) $Rh_s[Sn(n\text{-}C_4H_9)_2]y/SiO_2$, and (c, bottom) $\equiv SiOSnBu_3$.

**Table V.** Isomer Shift ($\delta$) and Quadrupole Splitting ($\Delta$) Mössbauer Parameters for $^{119}Sn$ in Surface Complexes and Molecular Analogues

| SOM complex or molecular analogue | $\delta$ (mm $s^{-1}$) | $\Delta$ (mm $s^{-1}$) | ref |
|---|---|---|---|
| $Sn(n\text{-}C_4H_9)_4/SiO_2$ (physisorbed) | 1.38 | 0 | this work |
| $Rh_s[Sn(n\text{-}C_4H_9)_2]/SiO_2$ | 1.4 | 1.4 | this work |
| $\equiv SiOSn(n\text{-}C_4H_9)_3$ | 1.4 | 2.7 | this work |
| $\equiv SiOSn(n\text{-}C_4H_9)_3$ | 1.3 | 2.8 | 31 |
| $Pt_4Sn(C_2H_5)_3/SiO_2$ | 1.29 | 3.16 | 49 |
| $PtSn/SiO_2$ | 1.84 | 0.68 | 50 |
| $Sn^{IV}(n\text{-}C_4H_9)_4$ | 1.35 | 0 | 40 |
| $Sn^{IV}(n\text{-}C_4H_9)_3(OEt)$ | 1.29 | 2.11 | 41 |
| $Sn^{IV}(n\text{-}C_4H_9)_3(SPh)$ | 1.46 | 2.06 | 42 |
| $Sn^{IV}(n\text{-}C_4H_9)_2(OEt)_2$ | 1.30 | 2.00 | 41 |
| $Sn^{IV}(n\text{-}C_4H_9)_2(OCH_2CH_2O)$ | 1.10 | 2.80 | 41 |
| $Sn^{II}(OCH_3)_2$ | 3.02 | 1.97 | 43 |
| $Sn^{II}Cp_2$ | 3.74 | 0.86 | 44–45 |
| $Sn^{II}(SbF_6)_2$ | 4.44 | 0 | 46 |

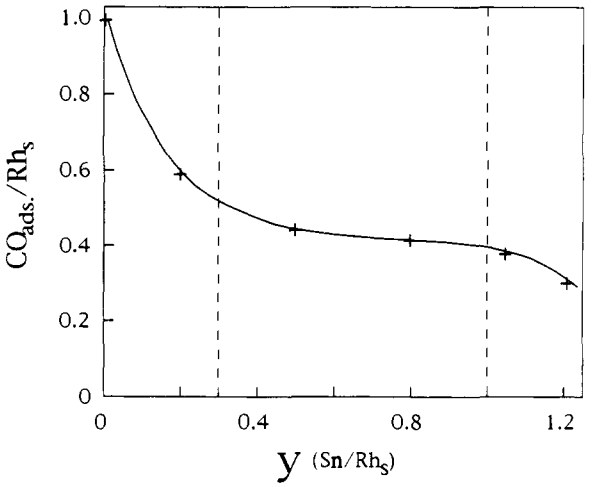


**Figure 8.** Volumetric determination of the amount of CO adsorbed on the catalyst described as $Rh_s[Sn(n\text{-}C_4H_9)_2]y/SiO_2$ as a function of $y$, $(Sn/Rh_s)$.

V). The value of the quadrupole splitting ($\Delta$ = 1.4 mm s$^{-1}$), which is related to the degree of symmetry of the electronic sphere around the Sn atom, describes an intermediate situation between X–Sn($n$-$C_4H_9$)$_3$ (X = oxygen atom or metal atom) ($\Delta > 2.7$ mm s$^{-1}$) and RhSn alloy ($\Delta$ = 0.68 mm s$^{-1}$).

**3.4.4. Volumetric Adsorption of CO.** Volumetric adsorption of CO has been used to quantify the number of Rh atoms still accessible to this probe molecule. Using this chemisorption method, one implicitly assumes that the surface structure and composition is not significantly perturbed by the probe molecule. Adsorption of CO at 298 K on several materials correspond to the formula $Rh_s[Sn(n\text{-}C_4H_9)_x]_y$ ($x$ = 2; $0 < y < 1$) gave the results depicted in Figure 8. In this figure, we report the correlation between $y$ (Sn/Rh$_s$) and the total amount of adsorbed CO (under an equilibrium pressure of 10 kPa). A sharp decrease of the amount of CO adsorbed occurs when the Sn/Rh$_s$ ratio increases from 0 to 0.3. A plateau is observed when the Sn/Rh$_s$ ratio increases from 0.3 to 1. It is interesting to note that even for values of $x$ as high as 1, approximately one-third of the Rh surface remains accessible to the CO molecule. This is a surprising result which will be discussed later.

**3.4.5. Infrared Spectroscopy of Adsorbed CO.** Infrared spectroscopy has been used to study the mode of coordination of CO on $Rh_s[Sn(n\text{-}C_4H_9)_2]/SiO_2$. Two bands are observed at 2023 and 1860 cm$^{-1}$ (Figure 3b). The high-frequency band is shifted to lower frequencies (36 cm$^{-1}$) compared to pure Rh, whereas the position of the bridging carbonyl band is almost unchanged. The fact that linear and bridged carbonyls are present in approximately the same intensity ratio compared to pure Rh clearly indicates that patches of accessible Rh atoms still exist on $Rh_s[Sn(n\text{-}C_4H_9)_2]/SiO_2$. When the solid was treated at 623 K under $H_2$, the resulting IR spectrum, after chemisorption of CO, does not contain any bands which could correspond to bridging CO. This result was the origin of the concept of site isolation.[7,47]

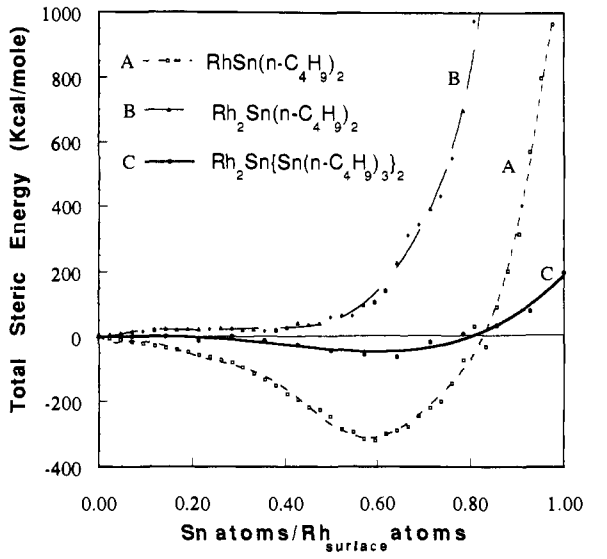


**Figure 9.** Computed total energy of various alkyltin fragments, models A, B, and C, on a cubooctahedral Rh particle as a function of coverage ($y$).

**Chart I**

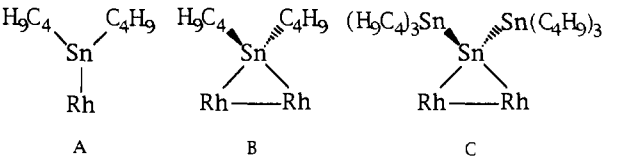


**3.4.6. Molecular Modeling.** In order to determine the maximum number of Sn($n$-$C_4H_9$)$_2$ fragments which can be reasonably accommodated on the Rh particle surface before steric hindrance becomes too high, we performed molecular modeling of the $Rh_s[Sn(n\text{-}C_4H_9)_2]_y/SiO_2$ catalyst using Sybyl software.[17]

Following the method of Van Hardeveld,[16] we assumed that the silica-supported Rh monometallic starting material can be represented by regular cubooctahedral particles about 0.13 nm in diameter. In this case the particle surface is composed only of (100) and (111) faces. The number of Rh atoms on each edge of the face is equal to 3. The total number of Rh atoms in the particle and on the surface are 55 and 40, respectively (dispersion of 0.73).

For the organometallic fragment grafted on the Rh surface, several models corresponding to an average of two butyl groups per Sn atom were considered (Chart I).

For the **first model** (model A, Chart I), only the steric hindrance from the butyl groups of the Sn($n$-$C_4H_9$)$_2$ fragment was taken into account. A Rh–Sn distance of 2.2 Å was assumed in order to keep the distance between the Sn atom and Rh surface consistent with the data obtained by EXAFS.[48] Additionally, the Sn was assumed to be trigonal for the sake of simplicity. Each Sn($n$-$C_4H_9$)$_2$ fragment was added to the Rh cubooctahedron using the following method: corner sites were filled first, followed by edges and finally faces. Fragments were added as symmetrically as possible. After each addition, an energy minimization was performed. A plot of total energy versus number of Sn($n$-$C_4H_9$)$_2$ is shown in Figure 9A. In the absence of significant strain due to the simple nature of the model, favorable van der Waals contacts cause the total energy to become negative. The total energy

(39) Wagner, C. D.; Riggs, W. M.; Davis, L. E.; Maulder, J. F.; Muilenberg, G. E. *Handbook of X-Ray Photoelectron Spectroscop*;, Perkin Elmer: Eden, MN.
(40) Davies, A. G.; Smith, P. J. In *Comprehensive Organometallic Chemistry*; Wilkinson, G.; Stone, F. G. A., Abel, E. W., Eds.; Pergamon: Oxford, 1982; Vol. 2, p 523.
(41) Smith, P. J.; White, R. F. M.; Smith, L. *J. Organomet. Chem.* **1972**, *40*, 341.
(42) Barbieri, R.; Sylvestry, A.; Lo Giudice, M. T.; Ruisi, G.; Musmeci, J. *J. Chem. Soc., Dalton Trans.* **1989**, 519.
(43) Harrison, P. G.; Stobar, S. R. *J. Chem. Soc., Dalton Trans.* **1973**, *940*.
(44) Harrison, P. G.; Zuckerman, J. J. *J. Am. Chem. Soc.* **1969**, *91*, 6885.
(45) Willamson, R. L.; Hall, M. B. *Organometallics* **1986**, *5*, 2142.
(46) Mallela, S. P.; Tomic, S. T.; Lee, K.; Sams, J. R.; Aubke, F. *Inorg. Chem.* **1986**, *25*, 2939.
(47) (a) Toolenaar, F. J.; Stoop, F.; Ponec, V. *J. Catal.* **1983**, *82*, 1. (b) Bastein, A. G.; Toolenaar, F. J.; Ponec, V. *J. Catal.* **1984**, *90*, 88. (c) Ichikawa, M.; Lang, A. J.; Shriver, D. T.; Sachtler, W. M. H. *J. Am. Chem. Soc.* **1985**, *107*, 7216.
(48) J. P. Candy et al., to be submitted for publication.

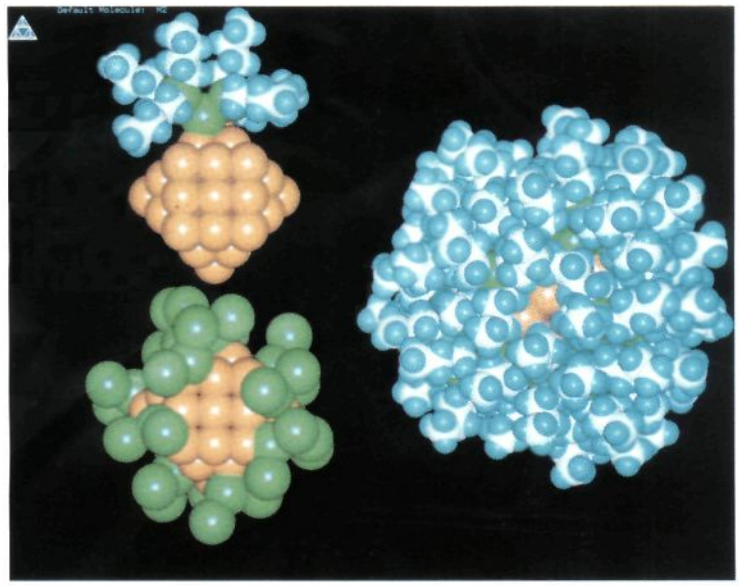

**Figure 10.** Representations of a 55-atom cubooctahedral Rh particle covered with $Sn[Sn(n\text{-}C_4H_9)_3]_2$ fragments, using van der Waals radii. Top left: particle with a $Sn(Sn(n\text{-}C_4H_9)_3)_2$ fragment grafted on an edge. Below left: same particle covered with 14 fragments of $Sn(Sn)_2$ coordinated to low coordination sites. Right: same particle covered with the butyl groups.

begins to increase as the number of $Sn(n\text{-}C_4H_9)_2$ groups exceeds 25 ($Sn/Rh_s = 0.63$). The increase becomes dramatic over 30 groups ($Sn/Rh_s = 0.75$). Addition of groups after a total of 36 is particularly unfavorable due to the fact that the additions are now to the (100) faces of the cubooctahedron.

For the **second model** (model B, Chart I), each $Sn(n\text{-}C_4H_9)_2$ fragment was bonded to two surface Rh atoms. The $Sn(n\text{-}C_4H_9)_2$ fragments were attached to the particle so that one Rh–Sn bond was always to a Rh corner atom and the other one always to an adjacent Rh edge atom. The groups were added as symmetrically as possible, with minimization after each group addition. Figure 9B shows the results of this minimization. As the number of $Sn(n\text{-}C_4H_9)_2$ groups on the particle increases, the total energy remains nearly the same until the number of groups approaches 24 ($Sn/Rh_s = 0.60$). At this point, two $Sn(n\text{-}C_4H_9)_2$ groups are bonded to each Rh corner atom. The steric energy increases dramatically once additional $Sn(n\text{-}C_4H_9)_2$ groups are added to the particle surface.

For the **third model** (model C, Chart I), it was assumed that two $Sn(n\text{-}C_4H_9)_3$ fragments were bonded to one Sn atom to form a $Sn[Sn(n\text{-}C_4H_9)_3]_2$ fragment. When such a surface structure is proposed, one implicitly assumes that some $Sn(n\text{-}C_4H_9)_4$ has undergone complete hydrogenolysis on low coordination sites of the surface, and the remaining alkyltin complex has undergone a less severe hydrogenolysis giving $Sn(n\text{-}C_4H_9)_3$ fragments which are then coordinated to the zerovalent Sn atoms. Such a model still corresponds to the average formula $Rh_s[Sn(n\text{-}C_4H_9)_2]$. This $Sn[Sn(n\text{-}C_4H_9)_3]_2$ fragment was then attached to two surface Rh atoms. The method of addition and energy minimization was identical with that of $Rh_2Sn(n\text{-}C_4H_9)_2$, however only 14 $Sn[Sn(n\text{-}C_4H_9)_3]_2$ fragments are necessary to achieve a $Sn/Rh_s$ ratio of 1. Figure 9C shows the results of this minimization. The steric energy begins to increase with the addition of the last two $Sn[Sn(n\text{-}C_4H_9)_3]_2$ fragments since each Rh corner atom already has a group bonded to it.

## 4. Discussion

**4.1. Starting Material.** In the course of this paper we have studied the selective hydrogenolysis of $Sn(n\text{-}C_4H_9)_4$ by silica-supported Rh. The first objective was to characterize as precisely as possible the starting Rh material. The metallic phase is composed of particles of zerovalent Rh regularly distributed on the silica surface with a narrow distribution of particle sizes centered around 1.4 nm. The size of these particles has been confirmed by chemisorption of CO and $H_2$.

**4.2. Reaction of $Sn(n\text{-}C_4H_9)_4$ with the Silica Support.** The second objective was to determine if $Sn(n\text{-}C_4H_9)_4$ reacts with the silica surface in the absence of metallic Rh particles. We have shown $Sn(n\text{-}C_4H_9)_4$ does not react significantly with the silica surface under the experimental conditions used in this work. This is consistent with other studies carried out in our laboratory[33] where we have shown by analytical methods ($^{13}C$ and $^{119}Sn$ NMR, Mössbauer spectroscopy, electron microscopy (STEM-EDAX)) that different conditions (423 K, 20 h) are necessary to obtain the well-defined surface compound $\equiv SiOSn(n\text{-}C_4H_9)_3$. At room temperature and up to 373 K, $Sn(n\text{-}C_4H_9)_4$ is simply physisorbed.

**4.3. Hydrogenolysis of $Sn(n\text{-}C_4H_9)_4$ with Silica-Supported Rh.** The third objective was to determine whether, in the presence of metallic Rh, hydrogenolysis occurs exclusively on the metallic particles. The $Sn(n\text{-}C_4H_9)_4$ is initially physisorbed onto the support, as seen by IR. This occurs by hydrogen bonding between the C–H groups and the silanols. Between 293 and 323 K, the complex migrates to the Rh surface where it quickly undergoes hydrogenolysis. Afterward, there is no evidence of physisorbed $Sn(n\text{-}C_4H_9)_4$ and no consumed silanols. Furthermore, no evidence of $\equiv SiOSn(n\text{-}C_4H_9)_3$ is seen by either Mössbauer spectroscopy of $^{13}C$ CP–MAS solid-state NMR (as long as the amount of $Sn(n\text{-}C_4H_9)_4$ added is less than one monolayer of $Rh_s$). Additionally, it was observed that the entire amount of the $Sn(n\text{-}C_4H_9)_4$ introduced on a $Rh/SiO_2$ sample is fixed on the solid at 373 K and cannot be extracted by *n*-heptane, whereas such extraction is quantitative with the silica alone.

Further evidence that an organometallic complex has formed exclusively on the Rh particles is obtained by several characterization methods. The STEM-EDAX experiments show that, provided that the amount of Sn introduced is lower than a monolayer of the $Rh_s$, the signal of Sn is always associated with the signal of Rh. No Sn signal was observed on the silica surface. Electron microscopy indicates that the average Rh particle size increases by a value of about 0.8 nm. Additionally, volumetric measurements of CO adsorption indicate that the amount of

(49) Vértes, C.; Talas, E.; Czako-Nagy, I.; Ryczkowski, J.; Göbölös, S.; Vértes, A.; Margitfalvi, J. *Appl. Catal.* **1991**, *68*, 149.
(50) Li, Y. X.; Klabunde, K. *J. Catal.* **1990**, *126*, 173.

adsorbed CO is inversely proportional to the amount of Sn present. All of this is consistent with the formation of a complex on the Rh particle, and not on the silica surface.

**4.4. Sequence of Reactions Occurring during the Hydrogenolysis of $Sn(n\text{-}C_4H_9)_4$.** The fourth objective was to understand the sequence of reactions which occurs between $Sn(n\text{-}C_4H_9)_4$ and the Rh surface. From the gas-phase evolution (Table IV and Figure 4) and the infrared studies (Figure 5), it is clear that the reaction proceeds stepwise via successive Sn–R bond cleavage:

$$y\mathrm{Sn}(n\text{-}\mathrm{C_4H_9})_4 + \mathrm{Rh_S/SiO_2} + z\mathrm{H_2}$$
$$(1)\downarrow$$
$$\mathrm{Rh_S[Sn}(n\text{-}\mathrm{C_4H_9})_3]_y/\mathrm{SiO_2}$$
$$(2)\downarrow$$
$$\mathrm{Rh_S[Sn}(n\text{-}\mathrm{C_4H_9})_2]_y/\mathrm{SiO_2}$$
$$(3)\downarrow$$
$$\mathrm{Rh_S[Sn}(n\text{-}\mathrm{C_4H_9})]_y/\mathrm{SiO_2}$$
$$(4)\downarrow$$
$$\mathrm{Rh_SSn}_y/\mathrm{SiO_2} + n\mathrm{C_4H_{10}}$$
$$(0 < y < 1)$$

Depending on the $Sn/Rh_s$ ratio ($y$), two situations can be observed. For a $Sn/Rh_s$ ratio of 0.3 to 0.53, the reaction seems to be continuous, resulting in various degrees of substitution of the remaining organometallic fragment. For a $Sn/Rh_s$ ratio of 0.71 to 0.96, there is a clear discontinuity in the curves of Figure 4. The plateau observed for a wide range of temperatures (75 K) indicates the selective formation of a relatively stable and well-defined surface organometallic fragment which has been formulated as $Rh_s[Sn(n\text{-}C_4H_9)_2]_y/SiO_2$. The presence of this fragment on the Rh surface does not inhibit the adsorption of CO in its linear and branched modes, indicating that patches of adjacent Rh atoms still exist. The fraction of Rh accessible to CO is ca. 30% of the starting surface of Rh.

Additional information can be deduced from the nature of the gases evolved (Table IV). For example, for a $Sn/Rh_s$ ratio lower than 0.53 and for temperatures up to 373 K butane is formed as the major product, while above 423 K only ethane is observed. The hydrogenolysis properties of Rh are progressively lost as coverage of Rh by the organometallic fragment increases. This suggests that the hydrogenolysis to form the organometallic complex may occur first selectively on the Rh atoms which are also selective for the hydrogenolysis of butane to ethane. This could represent a new method of selective poisoning of metallic surfaces by Sn atoms or Sn organometallic fragments.

**4.5. Possible Structure of $Rh_s[Sn(n\text{-}C_4H_9)_2]/SiO_2$.** The last objective of this work was to try to make a model of the possible structure of $Rh_s[Sn(n\text{-}C_4H_9)_2]/SiO_2$, which is a surprisingly stable surface organometallic complex and which also exhibits fascinating properties of chemoselectivity in the hydrogenation of olefinic aldehydes.[14]

Volumetric measurements, infrared data, and chemical analysis demonstrate that the overall formula of this complex is $Rh_s[Sn(n\text{-}C_4H_9)_2]/SiO_2$. From XPS data, all of the Rh atoms are in the Rh(0) state, the majority of the Sn atoms (75%) are in an oxidized form (II or IV), and the rest of the Sn atoms are in the zerovalent state. Mössbauer experiments also support the presence of Sn(IV). One can consider that in the case of a Sn–alkyl bond, Sn is formally oxidized. The presence of IR bands for both linear and bridging CO indicates that the accessible Rh surface atoms are not "isolated" from each other as in the alloy RhSn.[35]

Several models need to be considered in order to determine the best model for the surface organometallic complex. Let us first consider the simplest possible model, that of $RhSn(n\text{-}C_4H_9)_2$ (model A, Chart I). While this model is crude, it is useful because it shows us that the maximum number of $n$-butyl groups that can be accommodated on the Rh particle is between 30 and 36, which corresponds to a $Sn/Rh_s$ ratio of 0.71 to 0.86. Additionally, it shows us that the observed steric hindrance is due almost entirely to the $n$-butyl groups. Independent minimization of the Sn atoms shows that they can be easily accommodated on the Rh particle surface and that the unfavorable strain and van der Waals contacts are from the interactions between $n$-butyl groups.

A more realistic model can be proposed by assuming Sn is in a tetrahedral environment with two bonds to the Rh surface (model B, Chart I). However, calculations show that the model $Rh_2Sn(n\text{-}C_4H_9)_2$ can accommodate even fewer $n$-butyl groups, due to the fact that the tetrahedral environment is more restrictive than that of $RhSn(n\text{-}C_4H_9)_2$. The maximum number of Sn groups that can be accommodated with this model is between 22 and 26, which corresponds to a $Sn/Rh_s$ ratio of between 0.52 and 0.62.

Clearly, it is not possible to achieve a $Sn/Rh_s$ ratio of 1 with either of these two models. In order to accommodate enough $n$-butyl groups and give a $Sn/Rh_s$ ratio of 1, it is necessary to create a model which moves the $n$-butyl groups farther away from the Rh particle surface, while still maintaining a Sn/$n$-butyl ratio of 1 to 2 and keeping 40% of $Rh_s$ accessible to the CO probe molecule. The last model we suggest, $Rh_2Sn[Sn(n\text{-}C_4H_9)_3]_2$ (model C), is shown in Figure 9C. This model also agrees with the observation of ca. 25% of Sn(0) on the surface (XPS measurements). Calculations show that the steric crowding of this model at a $Sn/Rh_s$ ratio of 0.86 is only a fraction of that observed for the model $RhSn(n\text{-}C_4H_9)_2$. Additionally, a $Sn/Rh_s$ ratio of 1 can reasonably be achieved without major steric hindrance.

It is difficult at this stage to make a clear-cut choice between the various models. It is possible that a mixture of species are present. A model of the most likely situation for a $Sn/Rh_s$ ratio of 1 (model C, Figure 10) indicates that the particle of Rh is surrounded by a sphere of alkyl groups, leaving 40% of Rh atoms accessible to the reagents. This model suggests that, before reaching the surface Rh atoms, any incoming molecule will interact with these alkyl groups. Obviously, this represents a new generation of catalysts for which a better control of electronic and steric effects is possible.

**Acknowledgment.** CNRS is gratefully acknowledged for a Poste-rouge to Dr. Tim Shay. F. Lefebvre is also acknowledged for carrying out the NMR experiments, C. Leclerc for carrying out the electron microscope measurements, P. Bussière for carrying out the Mössbauer experiments, and P. Delichère and J. C. Bertholini for carrying out the XPS experiments.